Chromatin-immunoprecipitation reveals the PnPf2 transcriptional network controlling effector-mediated virulence in a fungal pathogen of wheat

Evan John, Karam B Singh, Richard P Oliver, Jessica L Soyer, Jordi Muria-Gonzalez, Daniel Soo, Silke Jacques, Kar-Chun Tan

Title: Chromatin-immunoprecipitation reveals the PnPf2 transcriptional network controlling effector-mediated virulence in a fungal pathogen of wheat.

Running title

PnPf2 regulation of virulence

Author names and affiliations:

Evan John[1,#,*], Karam B. Singh[1,2], Richard P. Oliver[3], Jessica L. Soyer[4], Jordi Muria-Gonzalez[1], Daniel Soo[1], Silke Jacques[1] and Kar-Chun Tan[1,#]

[1]Centre for Crop and Disease Management, Curtin University, Perth, Australia

[2]Agriculture and Food, Commonwealth Scientific and Industrial Research Organisation, Perth, Australia

[3]School of Biosciences, Nottingham University, Nottingham, United Kingdom

[4]Université Paris-Saclay, INRAE, UR BIOGER, 78850, Thiverval-Grignon, France

*Current address:

Institute of Plant and Microbial Biology, Academia Sinica, Taipei 11529, Taiwan

[#]Please direct author inquiries to:

Evan John - evan.john@curtin.edu.au

Kar-Chun Tan – Kar-Chun.Tan@curtin.edu.au

Abstract

The regulation of virulence in plant-pathogenic fungi has emerged as a key area of importance underlying host infections. Recent work has highlighted the role of transcription factors (TFs) that mediate the expression of virulence-associated genes. A prominent example is Pf2, a member of the Zn_2Cys_6 family of fungal TFs, where orthologues regulate the expression of genes linked to parasitism in several plant-pathogen lineages. These include PnPf2 which controls effector-gene expression in *Parastagonospora nodorum*, thereby determining the outcome of effector-triggered susceptibility on its host, wheat. PnPf2 is a promising target for disease suppression but the genomic targets, or whether other are regulators involved, remain unknown. This study used chromatin immunoprecipitation (ChIP-seq) and a mutagenesis analysis to investigate these components. Two distinct binding motifs connected to positive gene-regulation were characterised and genes directly targeted by PnPf2 were identified. These included genes encoding major effectors and other components associated with the *P. nodorum* pathogenic lifestyle, such as carbohydrate-active enzymes and nutrient assimilators. This supports a direct involvement of PnPf2 in coordinating virulence on wheat. Other TFs were also prominent PnPf2 targets, suggesting it also operates within a transcriptional network. Several TFs were therefore functionally investigated in connection to fungal virulence. Distinct metabolic and developmental roles were evident for the newly characterised PnPro1, PnAda1, PnEbr1 and the carbon-catabolite repressor PnCreA. Overall, the results uphold PnPf2 as the central transcriptional regulator orchestrating genes that contribute to virulence on wheat and provide mechanistic insight into how this occurs.

Importance

Fungal pathogens cause large crop losses worldwide and consequently much attention has focused on improving host genetic resistance to diseases. These pathogens use effectors, which require coordinated expression at specific stages of the pathogenic lifecycle, to manipulate the host plant metabolism in favour of infection. However, our understanding of the underlying regulatory network in coordination with other genes involved in fungal pathogenicity is lacking. The Pf2 TF orthologues are key players underpinning virulence and effector gene expression in several fungal phytopathogens, including *P. nodorum*. This study provided significant insight into the DNA-binding regulatory mechanisms of *P. nodorum* PnPf2, as well as further evidence that it is central to the coordination of virulence. In the context of crop protection, the Pf2 taxonomic orthologues present opportune targets in major fungal pathogens that can be perturbed to reduce the impact of effector triggered-susceptibility and improve disease resistance.

Keywords

Transcription factor, virulence, regulation, gene expression, orthologue

Abbreviations

Transcription factor (TF), DNA-binding domain (DBD), chromatin immunoprecipitation (ChIP), carbohydrate-active enzyme (CAZyme), amino acid (a.a), gene ontology (GO)

1. Background

The *Parastagonospora nodorum*-wheat interaction has become a model fungal-plant pathosystem to study the molecular virulence factors underpinning infection. The fungus produces small secreted effector proteins that selectively interact with host-receptors encoded by dominant susceptibility-genes (1, 2). These interactions occur in a gene-for-gene manner that causes 'effector-triggered susceptibility' in the host plant, quantitatively affecting the disease which manifests as septoria nodorum blotch. Several effectors acting in this manner have now been identified and characterised for their role in virulence (3–7). These studies have also described a consistent pattern: the expression of these genes is maximal two to four days after infection and then declines. Furthermore, expression levels can vary by the presence or absence of their matching wheat receptors, as well as by epistasis, whereby one effector gene causes suppression of another (8–10). Yet relatively little is known concerning the mechanisms governing the effector gene regulation. In particular, are there common or distinct regulatory pathways involved? Do these components specifically control effector gene expression, or co-regulate other metabolic and developmental pathways? New knowledge in this area could present suitable targets to suppress for disease control.

Many fungi possess a Zn_2Cys_6 transcription factor (TF) Pf2 that has been associated with the regulation of effector gene expression. One example is the AbPf2 orthologue in *Alternaria brassicicola* that is critical for virulence on *Brassica* spp. (11). Gene deletion of *AbPf2* resulted in the down-regulation of a number of effector like genes, as well as putative cell-wall degrading enzymes. In *P. nodorum*, at least two key effector genes, *ToxA* and *Tox3*, require PnPf2 t be expressed (12). An RNA-seq

93 analysis also revealed PnPf2 regulates many more putative effectors, CAZymes,
94 hydrolases/peptidases and nutrient transporters (13). The PtrPf2 orthologue in
95 *Pyrenophora tritici-repentis* controls *ToxA* expression and virulence on wheat, much
96 like for the homologous *ToxA* gene in *P. nodorum* (12). In *Leptosphaeria maculans*,
97 the causal agent of blackleg disease on *Brassica* spp., the LmPf2 orthologue also
98 regulates several effector genes, including *AvrLm4-7, AvrLm6,*
99 *AvrLm10A* and *AvrLm11*, as well as CAZyme expression (14).
100
101 The Pf2 orthologues can be traced across several Ascomycota fungal lineages
102 that include the Dothideomycetes, Leotiomycetes and Soradiomycetes (15). Gene-
103 deletion in the plant pathogens *Botrytis cinerea*, *Fusarium* spp., *Magnaporthe oryzae*
104 and *Zymoseptoria tritici* all suppressed fungal virulence as well as their capacity to
105 utilise alternative carbon sources (16–19). Analogous carbohydrate regulatory roles
106 have been attributed in the saprophytic fungi *Neurospora crassa* and *Trichoderma*
107 *reesei* (20, 21). In *N. crassa*, the putative orthologue Col-26 is a critical component
108 within a signalling-network that responds to glucose availability and promotes the
109 expression of CAZymes for plant cell-wall degradation (22–24). There is a strong
110 association between CAZyme gene content and plant-pathogenic lifestyles (25).
111
112 There are some key factors yet to be established among Pf2 orthologues. Which
113 DNA-regulatory elements are bound? Are Pf2-regulated genes directly targeted or is
114 their expression modulated by indirect factors? Are there other TFs intimately
115 connected with Pf2 regulation of virulence? The research presented here provides
116 such critical insight for PnPf2 in *P. nodorum*, and establishes its direct role in effector
117 expression and CAZyme regulation. A subsequent functional investigation of several

118 connected and directly targeted TFs provides further evidence for the central role held
119 by PnPf2 in the transcriptional network that orchestrates virulence in *P. nodorum*.
120

2. Results

2.1. PnPf2 possesses typical Zn_2Cys_6 TF domains and localises to the nucleus.

Conserved domains or distinguishing features were analysed in the 652 amino acid (a.a) PnPf2 protein. The Zn_2Cys_6 DNA binding domain was located N-terminally at a.a 9 to 54 with an overlapping nuclear localisation signal (NLS) (KKGPKGSR; a.a 51 to 58) (**Fig. 1A**). A 'fungal TF domain' was identified from a.a 223 to 294 within a conserved 'middle homology region' (a.a 104 to 320). These features are frequently observed in Zn_2Cys_6 TFs and have been linked to the modulation of TF activity (26, 27, 15). A structurally disordered domain, typically associated with post-translational modifications and intermolecular interactions (28), was also identified at the C-terminus of PnPf2. Together, these features suggested that PnPf2 possesses the typical functional domains underpinning DNA-binding Zn_2Cys_6 TF activity (26). Nuclear localisation of the C-terminally tagged PnPf2-GFP fusion protein was also observed (**Fig. 1B**). Along with the functional domains identified, this supported DNA-binding regulatory activity by PnPf2.

Fig. 1 HERE

2.2. Two direct PnPf2 target motifs are associated with gene-regulation

A chromatin immunoprecipitation (ChIP) analysis was used to define PnPf2-DNA binding *in situ*. The *Pf2-HA* (native promoter) and *Pf2-HA_OE* (overexpression promoter) strains expressing the 3x haemagglutinin (HA) tagged PnPf2-HA fusion protein retained PnPf2 function, in contrast to a *pf2-HA_KO* deletion control (**Text S1**). A ChIP-seq analysis was therefore undertaken using the *Pf2-HA* and *Pf2-HA_OE* strains to identify 'summits' within enriched 'peak' regions. Summits corresponded to the best estimate of PnPf2-DNA binding loci within the peaks (29). The *Pf2-HA* and *Pf2-HA_OE* samples provided complementary datasets; the overexpression mutant to compensate for lower *PnPf2* expression under culture conditions (13, 30) and broaden the DNA interactions captured. A total of 997 summits were obtained from the *Pf2-HA* dataset and 2196 from *Pf2-HA_OE*, corresponding to 740 and 1588 peak regions respectively. There were 588 shared peaks identified between the samples (**File S1**), indicating strong overlap between the predicted PnPf2-targeted regions. The *Pf2-HA_OE* dataset broadened the scope of putative binding sites. A quantitative PCR (qPCR) analysis was then undertaken on independently prepared ChIP DNA, comparing the *Pf2-HA* and *Pf2-HA_OE* samples to the *pf2-HA_KO* control. Fold-enrichment values relative to *pf2-HA_KO* strongly correlated with ChIP-seq summit -Log_{10}(Q-values), a proxy measure for PnPf2-DNA binding affinity, in both the *Pf2-HA* ($P < 0.01$ with Pearson's $r = 0.77$) and *Pf2-HA_OE* ($P < 0.01$ with Pearson's $r = 0.74$) datasets (**Text S1**). The high reproducibility across separate methodologies provided confidence in the robustness of ChIP-seq summit calls.

Text S1 HERE

File S1 HERE

Previous RNA-seq differential-expression analyses had identified an enriched consensus motif (5'-WMGGVCCGAA-3') in the promoter regions of both AbPf2 and PnPf2-regulated genes (11, 13). Despite harbouring the typical 'CGG' Zn_2Cys_6 binding triplet (26), an interaction with PnPf2 was not observed in a heterologous system, indicating regulatory cofactors may be required (31, 13). A search for DNA-regulatory elements that interact with PnPf2 from the ChIP-seq dataset identified two enriched motifs in the merged *Pf2-HA* and *Pf2-HA_OE* peak regions (**Fig. 2A**). The first motif designated as M1 (5'-RWMGGVCCGA-3') closely matches the consensus motif from AbPf2 and PnPf2-regulated gene promoters (11, 13). The second motif designated as M2 (5'-CGGCSBBWYYKCGGC-3') is novel for PnPf2, encompassing two copies of the canonical 'CGG' Zn_2Cys_6 binding triplets (26), separated by eight nucleotides. Interestingly, M2 matches the AmyR regulatory response element that was modelled in *A. nidulans* (32). Both M1 and M2 are close to the ChIP-seq summits for the *Pf2-HA* and *Pf2-HA_OE* datasets (**Fig. 2B**), suggesting they accurately reflected DNA-binding loci.

The previous RNA-seq analysis had defined genes positively or negatively-regulated by PnPf2 from their expression changes in the *PnPf2*-deletion mutant *pf2ko* relative to wildtype SN15 (13). These gene sets include the *in vitro* culture conditions that were replicated here for ChIP to maximise TF-DNA yields, as well as an early fungal infection stage *in planta* (72 hrs). Instances of M1 and M2 were then identified across the promoters of the positive (i.e. *pf2ko*-down) and negative (*pf2ko*-up) PnPf2-regulated gene sets (**File S2**). Both M1 and M2 were significantly enriched in the

positively-regulated gene promoter set only (**Fig. 2A**). This indicates both motifs correspond to cis-regulatory elements that induce, rather than repress, gene expression.

A novel approach here sought to detect specifically the PnPf2-motif interactions. This utilised a *dTomato* reporter gene fused to the promoter of SNOG_15417. The promoter was chosen to encompass a ChIP-seq peak region with both the M1 and M2 motifs for a gene that is positively-regulated by PnPf2 (**Fig. 2C**; **File S2**). Integration of the construct at a predefined genomic locus in the SN15 background permitted evaluation of the reporter-gene expression in the resultant strain (*p15417_M1M2*) in comparison with strains where the CGG triplets in M1 and/or M2 had been substituted (*p15417_m1M2*, *p15417_M1m2* and *p15417_m1m2*). Significantly reduced expression was observed in the strains where M1 had been mutated, indicating that it is a functionally important and direct PnPf2 target in the SNOG_15417 promoter (**Fig. 2C**). No significant expression change was detected where only the M2 motif was mutated.

Fig. 2 HERE

2.3. PnPf2 directly targets genes associated with the pathogenic lifestyle of *P. nodorum*

Genes with a ChIP-seq summit in their promoter region, considered a putative PnPf2 target, were cross-referenced with the *pf2ko* RNA-seq data analysis (**File S2**). There were 1286 targets identified from either ChIP-seq dataset, 484 of which were considered 'high-confidence' with a promoter summit in both *Pf2-HA* and *Pf2-HA_OE* (**Fig. 3A**). Of the 484 direct targets, 72 genes were positively-regulated in contrast to 6 negatively-regulated genes under the same *in vitro* conditions used for ChIP-seq. This indicates PnPf2 functions mainly as a positive regulator of gene expression. When expanded to also encompass PnPf2-regulated genes *in planta*, 93 were positively while 27 were negatively-regulated genes (**Fig. 3B**). Differential expression was not detected in the pf2ko mutant for 364 genes. This suggests other regulatory factors play a considerable role in their expression.

File S2 HERE

The characterised effector genes present in *P. nodorum* SN15, *ToxA, Tox1, Tox3* and *Tox267* (7), plus 29 other effector-like genes whose expression was altered in the *pf2ko* mutant, were assessed for evidence of direct regulation by PnPf2. Two distinct ChIP-seq summits were identified in the bi-directional *Tox3* promoter (**Fig. S1**). Both the upstream gene (i.e. SNOG_08982, encoding a protein disulphide-isomerase) and downstream gene (*Tox3*) are positively regulated by PnPf2. A ChIP-seq summit was also identified in the *Tox1* promoter, but only from the *Pf2-HA_OE* dataset (**Fig. S1**). Unlike Tox3, Tox1 necrosis-inducing activity is still detected in the *pf2ko* background (12), indicating the summit may represent a weak enhancer element. The

234 *ToxA* gene is only expressed during infection but in a PnPf2-dependent manner. A
235 weak promoter summit was observed despite multiple instances of the M1 motif,
236 suggesting another factor(s) is required to facilitate PnPf2-DNA binding that was
237 absent under the ChIP-seq experimental conditions. No distinct PnPf2 summit was
238 observed in the promoter of *Tox267*, whose expression is not significantly altered in
239 the *pf2ko* mutant, although two instances of M1 were identified >1000 bp upstream
240 (**Fig. S1**). In total, 11 of the 29 PnPf2-regulated effector-like genes showed evidence
241 of direct PnPf2-promoter binding through ChIP-seq summits (**Table S1-A**).
242
243 **Fig. S1 HERE**
244

A gene-ontology (GO) enrichment and network analysis was then carried out to identify major functional gene classes that are directly regulated by PnPf2. Five distinct groups representing TFs, redox molecules, CAZymes, cell-signalling molecules and nutrient transporters were significantly enriched among the GO networks (**Fig. 3C-D**). The enrichment of CAZymes, redox molecules and nutrient transporters is consistent with enriched functional GO classes that were observed for the *pf2ko* differentially expressed genes (13). In contrast, the TFs and cell-signalling molecules were not enriched, indicating they could be tightly controlled by redundant pathways in addition to PnPf2. Nevertheless, it was striking that TF genes were particularly enriched in the high-confidence set of 484 targets (**Fig. 3C-D**). They made up 9.1% of these genes in contrast to 3.5% of the total genes annotated for SN15. Five TFs were directly targeted and positively regulated, providing a direct connection with PnPf2 in the regulation of virulence (**Table S1-B**).

Fig. 3 HERE

Table S1 HERE

2.4. PnPf2 is the central transcriptional regulator of host-specific virulence

The identification of TFs as major PnPf2 targets prompted a functional exploration of other TFs with a putative intermediate role in regulating virulence. Three directly-regulated TF genes were therefore targeted for deletion where orthologues had virulence-associated roles (**Table 1**). These included SNOG_03490 (*PnPro1*), SNOG_04486 (*PnAda1*) and SNOG_08237. Two additional TF-encoding genes were simultaneously investigated. This included SNOG_08565, identified in the PnPf2 lineage of fungal TFs (15) suggesting a possible common evolutionary origin. It also included SNOG_03067 (*PnEbr1*), which is co-expressed with *PnPf2, ToxA*, *Tox1* and *Tox3* high during early infection (**Fig. S2**), suggesting a similarly important role in disease.

Fig. S2 HERE

Gene deletion strains for the five TFs were phenotypically characterised in comparison to wildtype SN15 and *pf2ko*. The *pro1_KO*, *ada1_KO* and *ebr1_KO* deletion mutants presented distinct phenotypic abnormalities (**Fig. 4**). The *pro1_KO* mutants were abolished in their ability to form pycnidia and sporulate both during infection and on nutrient-rich agar. However, vegetative growth was expansive in both conditions (**Fig. 4A-B**), suggesting PnPro1 acts to suppress hyphal development. Although *PnPro1* is positively-regulated by PnPf2, there was no distinct phenotypic overlap with the *pf2ko* mutant. The *ada1_KO* mutant was significantly reduced in virulence on detached leaves (**Fig. 4A-B**). Dark brown discolouration at the site of infection suggested a hypersensitive response had contained the infection. We also

observed an increased susceptibility to oxidative (H_2O_2) stress for *ada1_KO* mutants similar to *pf2ko*. Furthermore, sporulation was reduced in *ada1_KO* relative to SN15 (**Fig. 4C-E**). The *ebr1_KO* mutants exhibited vegetative growth defects with an uneven growth perimeter around the colony edges coinciding with perturbed virulence (**Fig. 4A-B**). Similar hyphal-branching defects were described following deletion of *PnEbr1* orthologues in *Fusarium* spp. (33, 34). Interestingly, the *ebr1_KO* mutants were also susceptible to H_2O_2 stress at a level comparable to *pf2ko* and *ada1_KO*. Furthermore, pycnidia were abnormally developed, although still viable for the production of conidia, but were not detected on infected leaves (**Fig. 4C-D**). We did not observe morphological or virulence defects for the *08237_KO* or *08565_KO* mutants (**Text S2**) which were not investigated in further detail.

Fig. 4 HERE

During the course of this study the carbon-catabolite repressor (CCR) element was modelled as the binding site for the Cre-1 TF that suppresses CAZyme expression in *N. crassa* (22). We noted this was near identical to a motif (5'-RTSYGGGGWA-3') that is also enriched in PnPf2-regulated gene promoters (13) but not identified from the ChIP-seq peaks. Since Cre-1 orthologues are conserved CCR regulators in filamentous fungi (35, 36), and since the CCR element is also enriched in PnPf2 regulated gene promoters, a putative Cre-1 orthologue (PnCreA) was investigated in *P. nodorum* to identify common regulatory pathways with PnPf2. Both *PnCreA* overexpression and gene-deletion mutants (*CreA_OE* and *creA_KO*) were created and then investigated alongside *pf2ko* and a *PnPf2* overexpression mutant (*Pf2_OE*). Despite clear phenotypic-growth abnormalities (**Fig. 5**), neither the *CreA_OE* nor

313 *creA_KO* mutants exhibited virulence defects on wheat leaves (**Text S2**). The
314 *creA_KO* strain was enhanced in starch utilisation (**Fig. 5**), an indicator substrate for
315 CCR activity (37). In contrast, there was a moderate reduction of *pf2ko* to utilise starch,
316 similar to observations in other fungal *PnPf2*-orthologue mutants (17, 19, 21). These
317 results support contrasting roles between PnCreA and PnPf2 for the regulation of
318 some CAZyme-related genes.
319
320 **Fig. 5 HERE**
321
322 **Text S2 HERE**
323
324 **Table 1 HERE**
325

3. Discussion

Prior to this research, PnPf2 had been identified as an important regulator of *P. nodorum* virulence on wheat (12, 13), but important details and mechanistic insights were missing. We sought to take further steps and establish the DNA-binding elements targeted by PnPf2 and identify genes that were directly under its direct regulation. Two distinct regulatory motifs M1 and M2 were identified and linked to positive gene-regulation by PnPf2. M1 was strikingly similar to an enriched sequence in AbPf2 positively-regulated gene promoters (11), possibly representing a conserved Pf2 binding mechanism. It will be pertinent to explore this motif as a regulatory target for other fungal Pf2 orthologues (11–14, 16–21). Interestingly, the M2 motif matches the extensively characterised AmyR regulatory-response element in *A. nidulans* (38, 32). Polysaccharide metabolism has long been established as a regulatory function for AmyR (39, 40). Therefore, some shared regulatory pathways likely exist with Pf2 orthologues given the evidence for at least one conserved binding mechanism. However, there are major a.a polymorphisms between AmyR and Pf2 orthologues at the Zn_2Cys_6 DNA-binding domain (15) and M1 has not been reported as an AmyR target despite extensive motif investigation (38, 32). It is therefore conceivable that M1 is a regulatory binding element unique to Pf2 orthologues and therefore useful to identify putative direct targets such as *ToxA* in *P. nodorum.*

The ChIP-seq PnPf2-DNA binding dataset also facilitated the identification of *P. nodorum* genes under direct PnPf2 regulation. Among these genes is the *Tox3* effector and the adjacent gene, SNOG_08982, encoding a protein disulphide isomerase. This class of protein catalyses cysteine-cysteine bond formation which has been connected to fungal effector protein production (41). Therefore, it would be worth

exploring any involvement of SNOG_08982 in the post-translational modification of Tox3 and other effectors. PnPf2 binding was also detected in the *Tox1* promoter. A partial reduction in *Tox1* expression was reported in the *pf2ko* mutant (13), indicating PnPf2 is not essential but enhances expression under favourable conditions. *ToxA* is only expressed *in planta,* but is PnPf2 dependent (12). Despite multiple instances matching the M1 motif, there was little evidence for PnPf2-*ToxA* promoter binding, suggesting chromatin inaccessibility or the absence of essential binding-cofactors under the ChIP culture conditions. Direct PnPf2 regulation of *Tox267* was not evident. The other recently-cloned effector gene *Tox5* is not present in the SN15 isolate used in this study, but is homologous to *Tox3* may be under PnPf2 control (6). Nevertheless, several other effector-like genes were identified as direct PnPf2 targets (**Table S1-A**). Importantly this analysis provided strong evidence that PnPf2 is a key direct-regulator of effectors, the major *P. nodorum* virulence factors in the lifestyle of this pathogen.

Evidence for regulation of effector expression has been reported for another *P. nodorum* TF PnCon7 (42), yet its apparent requirement for fungal viability renders it difficult to investigate a precise functional role. Here, several novel TFs were functionally investigated based on their connection to PnPf2 (**Table 1**). We did not observe any change in the necrosis-inducing activity on wheat of fungal culture filtrates derived from the respective mutants. However, developmental virulence roles, including oxidative stress tolerance and hyphal development, were identified for *P. nodorum* PnAda1 and PnEbr1. It is possible that the direct regulation of PnAda1 by PnPf2 contributes to the susceptibility to oxidative stress also identified in the *pf2ko* mutant. The PnCreA orthologue of *N. crassa* Cre-1 was also investigated, following the striking observation that the *N. crassa* Cre-1 CCR element (5′-TSYGGGG-3’) was

enriched in PnPf2-regulated gene promoters (13). Furthermore, Cre-1 and the PnPf2 orthologue Col-26 are both key components of a transcriptional network controlling CAZyme production in *N. crassa* (22–24, 43). Here, the *creA_KO* strain displayed an enhanced capacity to utilise starch, which was moderately impaired in the *pf2ko* mutant (**Fig. 5**). This indicates PnCreA and PnPf2 shared a similar function to the respective *N. crassa* orthologues (21). Surprisingly however, despite vegetative growth abnormalities on agar, there was no distinct change in the virulence profile of either the *creA_KO* or *CreA_OE* mutants (**Text S2**). We also failed to detect the CCR element in the promoters of *ToxA*, *Tox1*, *Tox3* or *Tox267* (**File S2**). This suggests that the regulation of host-specific virulence factors critical for *P. nodorum* infection are not subject to CCR by PnCreA.

This investigation, along with previous TF studies in *P. nodorum* (44, 45, 12, 42), indicate PnPf2 is central to the transcriptional-regulatory network controlling virulence, for which a tentative model is proposed (**Fig. 6**). Having expanded our understanding, it also raised some key questions. For many genes directly targeted by PnPf2, differential expression in *pf2ko* has not been observed (364 of 484 high-confidence targets). Such discrepancies are also reported in ChIP-seq experiments on filamentous fungi (**Table S2**). One aspect to consider is that functional TF binding requires specific cofactors/coregulators before gene expression is eventually modulated (46, 47). Furthermore, TF-DNA interactions can be redundant or non-functional (48–50). It is therefore plausible that many binding sites are transiently occupied by PnPf2 in this manner, acting as a biological sink. A change in the epigenetic landscape, for example during growth *in planta*, could open up genomic regions for which PnPf2 exhibits a high affinity and then actively binds. Performing

PnPf2 ChIP during early infection will likely prove highly useful in this regard if sufficient fungal material can be obtained. ChIP-seq targeting histone marks specific for euchromatin or heterochromatin under infection conditions, or methylation-sensitive sequencing are alternatives to provide insight into the genome accessibility of PnPf2 (14, 51–53). The identification of both the M1 and M2 motifs carrying alternatively oriented 'CGG' triplets, typical of Zn_2Cys_6 monomers (26), was suggestive of PnPf2 dimerisation with other Zn_2Cys_6 TFs. However, deletion of the putative ancestral PnPf2 homologue SNOG_08565 did not provide any phenotypic response that would indicate a connection. Therefore, future investigations will do well to explore these interactions, for example through co-immunoprecipitation/affinity purification analysis or a yeast-2-hybrid screen, to delineate PnPf2-DNA binding mechanisms. Functional investigation of the PnPf2 'middle homology region' and C-terminal disordered region may also provide insight into the upstream signalling pathways that activate or repress PnPf2 activity through these domains.

To conclude, this study presents direct evidence of DNA binding in a Pf2 orthologue, where virulence-regulatory functions are consistently observed in phytopathogenic fungi. In *P. nodorum*, PnPf2 is central to the transcriptional regulation of virulence and directly controls effector expression. The current research on PnPf2 now provides a platform to further investigate its signalling pathways and molecular interactions that could be inhibited for targeted disease control.

Fig. 6 HERE

Table S2 HERE

4. Materials and methods

4.1. Annotations and PnPf2 domain analysis

The *P. nodorum* annotated genome for the reference isolate SN15 (54) was used consistent with annotations in the previous RNA-seq analysis (13). The PnPf2 polypeptide sequence was submitted to Interproscan (Release 82.0) for Interpro and Conserved-Domain-Database domain identification (55). NLStradamus was used to predict the nuclear localisation signal (56). The disordered region was predicted using IUPRED2A (28).

4.2. Generation and assessment of fungal mutants

The molecular cloning stages, the constructs generated and diagrammatic overview of the final transformed *P. nodorum* mutants generated in this study are detailed in **Text S3**. The respective primers designed for fragment amplification and/or screening are outlined in **File S3**. Fungal mutants used in this study are summarised in **Table 2**. Their phenotypic and gene-expression analysis procedures are also described in **Text S3.**

Table 2. HERE

Text S3 HERE

File S3 HERE

4.3. Chromatin immunoprecipitation sample preparation

The *Pf2-HA*, *Pf2-HA_OE* and *pf2-HA_KO* strains were prepared following 3 days standardised growth in 100 mL Fries3 liquid medium (**Text S3**). Prior to harvesting, a 5 mL crosslinking solution (10% w/v formaldehyde, 20 mM EDTA and 2 mM PMSF dissolved in 50 mM NaOH) was added with continuous shaking at 100 rpm for 10 min. To this, 5 mL quenching solution (1.25 M glycine) was added before another 10 min shaking. Whole protein extracts were then obtained as described (**Text S3**) with modifications for ChIP. The 50 mM Tris was replaced with 50 mM HEPES in the lysis buffer while gentle rotation of the resuspended fungal material was replaced by eight rounds of sonication using a Bandelin (Berlin, Germany) UW3100+SH70+MS73 tip sonicator to fragment the fungal DNA (set at 15 sec on/off with 60% amp and 0.8 duty cycle). Samples were held in an ice block during sonication. The supernatant was then retrieved from two rounds of centrifugation (5000 g, 4 ^{o}C for 5 min). A 100 µL aliquot of the supernatant was reserved as an 'input control' against which ChIP samples were to be normalised. A 1000 µL aliquot was then precleared for immunoprecipitation by gently rotating with 20 µL Protein A dynabeads (10001D - Thermofisher, Waltham, Massachusetts) for 1 hr at 4 ^{o}C. The supernatant was then retrieved and incubated with 2.5 µg anti-HA polyclonal antibody (71-5500 - Thermofisher) for 16 hrs at 4 ^{o}C. Another 20 µL Protein A dynabeads were then added and gently rotated for 2 hrs at 4 ^{o}C. The dynabeads were then retrieved and washed twice with 1mL ice-cold lysis buffer, once with high-salt buffer (lysis buffer + 500 mM NaCl), once with LiCl buffer (250 mM LiCl, 10 mM Tris-HCl, 1 mM EDTA, 0.5% NP40 and 0.5% NaDOC) and once with TE buffer (10 mM Tris-HCl, 1 mM EDTA, pH 8). Samples were then incubated in a shaking incubator for 10 min (300 rpm, 65 ^{o}C) with 200 µL elution buffer (0.1 M $NaHCO_3$, 10 mM EDTA and 1% SDS) before

transferring the supernatant to a fresh tube. The input control was also supplemented with 100µL elution buffer at this stage and 8 µL NaCl solution (5 M) was added to both samples before de-crosslinking for 16 hrs at 65 ºC. To these samples, 200 µL of H_2O and 100 µg RNAse A (QIAGEN, Hilden, Germany) were added before incubating for 1 hr at 65 ºC. Ten µg Proteinase K (Sigma-Aldrich, St. Louis, Missouri) was then added before incubating a further 1 hr at 50 ºC.

For ChIP-qPCR, DNA (for both the *Pf2-HA*, *Pf2-HA_OE* and *pf2-HA_KO* ChIP and input control samples) was recovered from Proteinase K treated samples using the GenElute PCR purification kit (Sigma-Aldrich).

For ChIP-seq analysis, DNA (for both *Pf2-HA* and *Pf2-HA_OE* ChIP and input control samples) was purified from the Proteinase K treated samples by mixing in 1 volume (400 µL) of phenol:chloroform. This was centrifuged for 5 min at 16000 g and the aqueous phase retrieved. To this, 400µL chloroform was added, mixed and spun (16000 g 5 min) before 350 µL of the aqueous phase was transferred to a fresh tube. 35 µL sodium acetate (3 M, pH 5.2) was added with 1 µL of glycogen (20mg/mL). Samples were mixed by inversion and 1 mL 100% ethanol added before precipitation at -80 ºC for 1-2 hrs. Pellets were retrieved by spinning 16000 g for 10 min at 4 ºC, then washed in 1 ml of ice-cold 70% ethanol before drying and resuspension in 30 µL Tris-Cl (10 mM).

Two independent DNA preparations for each sample (i.e. the ChIP and input samples for both *Pf2-HA* and *Pf2-HA_OE*), beginning with the fungal growth stage in Fries3 broth, were pooled to ensure sufficient DNA was obtained for generating ChIP-

seq libraries. The pooled DNA was measured using a Tapestation system (Agilent, Santa Clara, California). 10 ng of each sample was processed using the TruSeq ChIP Library Preparation Kit (Illumina, San Diego, California). Libraries were size-selected (100-300 bp) and split across four separate lanes for sequencing in a NextSeq 500 sequencer (Illumina) to obtain 2 x 75 bp paired-end reads (Australian Genome Research Facility, Melbourne, Australia).

4.4. ChIP-seq analysis

An overview of the following data analysis pipeline from QC of raw reads through to genome mapping, ChIP-seq peak/summit calling, target gene prediction, ChIP-qPCR validation, GO enrichment analysis and motif position-weight-matrix (PWM) modelling **Text S1**.

4.4.1. Raw read filtering, mapping and peak/summit calling

Raw reads were checked using FASTQC (Version 0.11.9) (57) and the adapter sequences were trimmed using Cutadapt (Version 1.15) along with nucleotides where the Illumina quality scores were below 30 (58). Optical duplicates were then removed using the 'dedupe' option in Clumpify (version 1.15) from the BBTools package (59). Reads were subsequently mapped to the SN15 genome (54) using BWA-MEM (60). Reads mapping to a single locus as the best match (primary alignments) were retained for downstream analysis and the datasets from sample libraries originally split across the NextSeq lanes were merged using SAMtools (Version 1.10) to produce the final mapped-read datasets (61). MACS (Version 2.2.7.1) was used for calling enriched regions (i.e. peaks) and summits (highest nucleotide point or points within peak regions) from ChIP sample reads relative to the input samples (for *Pf2-HA* and *Pf2-*

HA_OE). A Q-value peak enrichment threshold of 0.01 was used and the BAMPE option utilised to assess read depth from cognate pairs (62, 63). Paired read lengths from the cognate pairs were assessed using Deeptools 'bamPEFragmentSize' (Version 3.3.0) to verify they corresponded to 100-300 bp size selected fragments (64).

4.4.2. Modelling binding-site motifs

The overlapping peak regions identified from the *Pf2-HA* and *Pf2-HA_OE* samples were merged using MAnorm (65) to create a consensus set of enriched peak regions containing the putative PnPf2 binding sites. From this set, overrepresented PWMs up to 20 bp long were modelled with MEME (version 5.1.1) (66, 67). For the resulting PWMs, 500 bp genomic regions centred at ChIP-seq summits were extracted and analysed using CentriMo (Version 5.1.1) to verify that the motif instances were also centred at the respective summits for both the *Pf2-HA* and *Pf2-HA_OE* samples (68). Gene promoters (spanning annotated transcription start sites to the nearest upstream gene feature or 1500 bp) with ≥ 1 occurrence of each motif were determined using FIMO (69). These were cross-referenced with the differentially expressed genes (i.e. expressed significantly up or down in *pf2ko* relative to SN15) defined in a previous RNA-seq analysis (13). Fisher's exact test with Bonferroni corrected P-values (70) was used to identify *pf2ko* differentially expressed gene-promoter sets significantly enriched ($P_{adj} < 0.01$) for the respective motifs vs the background rate in SN15.

4.4.3. PnPf2 target gene-promoter analysis

Genes targeted by PnPf2 were determined based on the proximity of summits to annotated genes, which were identified using ChIPseeker (Version 1.24.0) (71).

549 Genes with ≥1 summit falling within their promoter region from the *Pf2-HA* or *Pf2-*
550 *HA_OE* datasets were considered PnPf2 targets. High-confidence PnPf2 targets
551 corresponded to genes with a promoter summit in *Pf2-HA* and *Pf2-HA_OE*. ChIP-
552 qPCR was then undertaken to verify that the ChIP-seq peak regions in *Pf2-HA* and
553 *Pf2-HA_OE* would also correlate with quantitative enrichment against the *pf2-HA_KO*
554 control strain. Quantitative PCR primer pairs (**File S3**) were designed to flank ChIP-
555 seq summits in a selection of gene promoters (*ToxA*, *Tox1*, *Tox3*, SNOG_03901,
556 SNOG_04486, SNOG_12958, SNOG_15417, SNOG_15429, SNOG_16438,
557 SNOG_20100 and SNOG_30077) and a selection of non-summit control regions (*Act1*
558 and SNOG_15429 coding sequences and the TrpC terminator). The 'input %' values
559 were calculated for each sample using the method described previously (72) and used
560 to calculate fold-differences (normalised to *Act1*) for *Pf2-HA* and *Pf2-HA_OE* relative
561 to the *pf2-HA_KO* control for comparison with the *Pf2-HA* and *Pf2-HA_OE* $-\text{Log}_{10}$(Q-
562 values) at the respective ChIP-seq summit loci. Pearson's correlation coefficient was
563 calculated for the ChIP-qPCR fold-difference and ChIP-seq $-\text{Log}_{10}$(Q-values) at the
564 respective loci and used as the test statistic to assess whether the association was
565 significant (SPSS version 27.0).
566
567 The PnPf2 target genes were cross-referenced with the *pf2ko* expression
568 patterns (expressed significantly up or down in *pf2ko*) defined previously (13) to link
569 direct binding with the modulation of gene expression. The SN15 effector-like genes
570 annotated previously (13) were compiled among the PnPf2 targets. Annotated
571 homologues were identified from the corresponding records in UniProt (release
572 2020_05) (73). Both the high-confidence and total PnPf2 target-gene sets were then
573 used for GO enrichment/network analysis using the SN15 GO annotations defined

574 previously (13). The 'enricher' function in the Clusterprofiler package (Version 3.16.0)
575 (74) was invoked to identify the overrepresented GO classes ($P < 0.01$) in PnPf2
576 targets.
577
578 ### 4.5. Data availability statement
579 The ChIP-seq reads are available under BioProject ID: PRJNA824526,
580 corresponding to BioSamples SAMN27406642 (*Pf2-HA* strain) and SAMN27406643
581 (*Pf2-HA_OE* strain).
582
583 ## 5. Acknowledgements
584 This study was supported by the Centre for Crop and Disease Management, a joint
585 initiative of Curtin University (https://www.curtin.edu.au/) and the Grains Research and
586 Development Corporation (https://grdc.com.au/) under the research grant CUR00023
587 Project F3 awarded to KCT). EJ was supported by an Australian Government
588 Research Training Program Scholarship (https://www.dese.gov.au/) administered
589 through Curtin University (https:// www.curtin.edu.au/). The funders had no role in
590 study design, data collection and interpretation, or the decision to submit the work for
591 publication.
592
593 We would like to acknowledge Dr. Carl Mousley for helpful suggestions relevant to
594 ChIP-seq motif validation, Dr. Darcy Jones for bioinformatics advice and support, as
595 well as Johannes Debbler for assistance with molecular cloning.

6. References

1. McDonald MC, Solomon PS. 2018. Just the surface: advances in the discovery and characterization of necrotrophic wheat effectors. Current Opinion in Microbiology 46:14–18.

2. Kanyuka K, Igna AA, Solomon PS, Oliver RP. 2022. The rise of necrotrophic effectors. New Phytologist 233:11–14.

3. Friesen TL, Stukenbrock EH, Liu Z, Meinhardt S, Ling H, Faris JD, Rasmussen JB, Solomon PS, McDonald BA, Oliver RP. 2006. Emergence of a new disease as a result of interspecific virulence gene transfer. 8. Nature Genetics 38:953–956.

4. Liu Z, Faris JD, Oliver RP, Tan K-C, Solomon PS, McDonald MC, McDonald BA, Nunez A, Lu S, Rasmussen JB, Friesen TL. 2009. SnTox3 acts in effector triggered susceptibility to induce disease on wheat carrying the *Snn3* gene. PLOS Pathogens 5:e1000581.

5. Liu Z, Zhang Z, Faris JD, Oliver RP, Syme R, McDonald MC, McDonald BA, Solomon PS, Lu S, Shelver WL, Xu S, Friesen TL. 2012. The cysteine rich necrotrophic effector SnTox1 produced by *Stagonospora nodorum* triggers susceptibility of wheat lines harboring *Snn1*. PLOS Pathogens 8:e1002467.

6. Kariyawasam GK, Richards JK, Wyatt NA, Running KLD, Xu SS, Liu Z, Borowicz P, Faris JD, Friesen TL. 2022. The *Parastagonospora nodorum* necrotrophic effector SnTox5 targets the wheat gene Snn5 and facilitates entry into the leaf mesophyll. New Phytologist 233:409–426.

7. Richards JK, Kariyawasam GK, Seneviratne S, Wyatt NA, Xu SS, Liu Z, Faris JD, Friesen TL. 2022. A triple threat: the *Parastagonospora nodorum* SnTox267 effector exploits three distinct host genetic factors to cause disease in wheat. New Phytologist 233:427–442.

8. Phan HTT, Rybak K, Furuki E, Breen S, Solomon PS, Oliver RP, Tan K-C. 2016. Differential effector gene expression underpins epistasis in a plant fungal disease. The Plant J 87:343–354.

9. Peters-Haugrud AR, Zhang Z, Richards JK, Friesen TL, Faris JD. 2019. Genetics of variable disease expression conferred by inverse gene-for-gene interactions in the wheat-*Parastagonospora nodorum* pathosystem. Plant Physiology 180:420–434.

10. John E, Jacques S, Phan HTT, Liu L, Pereira D, Croll D, Singh KB, Oliver RP, Tan K-C. 2022. Variability in an effector gene promoter of a necrotrophic fungal pathogen dictates epistasis and effector-triggered susceptibility in wheat. PLOS Pathogens 18:e1010149.

11. Cho Y, Ohm RA, Grigoriev IV, Srivastava A. 2013. Fungal-specific transcription factor *AbPf2* activates pathogenicity in *Alternaria brassicicola*. The Plant J 75:498–514.

12. Rybak K, See PT, Phan HTT, Syme RA, Moffat CS, Oliver RP, Tan K-C. 2017. A functionally conserved Zn2Cys6 binuclear cluster transcription factor class regulates necrotrophic effector gene expression and host-specific virulence of two major Pleosporales fungal pathogens of wheat. Mol Plant Pathol 18:420–434.

13. Jones DAB, John E, Rybak K, Phan HTT, Singh KB, Lin S-Y, Solomon PS, Oliver RP, Tan K-C. 2019. A specific fungal transcription factor controls effector gene expression and orchestrates the establishment of the necrotrophic pathogen lifestyle on wheat. 1. Sci Rep 9:1–13.

14. Clairet C, Gay EJ, Porquier A, Blaise F, Marais CL, Balesdent M-H, Rouxel T, Soyer JL, Fudal I. 2021. Regulation of effector gene expression as concerted waves in *Leptosphaeria maculans*: a two-players game. BioRxiv 2021.12.15.472773.

644 15. John E, Singh KB, Oliver RP, Tan K-C. 2021. Transcription factor lineages in plant-
645 pathogenic fungi, connecting diversity with fungal virulence. Fungal Genetics and
646 Biology In press.

647 16. Chung H, Choi J, Park S-Y, Jeon J, Lee Y-H. 2013. Two conidiation-related
648 Zn(II)2Cys6 transcription factor genes in the rice blast fungus. Fungal Genet Biol
649 61:133–141.

650 17. Oh M, Son H, Choi GJ, Lee C, Kim J-C, Kim H, Lee Y-W. 2016. Transcription factor
651 ART1 mediates starch hydrolysis and mycotoxin production in *Fusarium graminearum*
652 and *F. verticillioides*. Mol Plant Pathol 17:755–768.

653 18. Habig M, Bahena-Garrido SM, Barkmann F, Haueisen J, Stukenbrock EH. 2020. The
654 transcription factor Zt107320 affects the dimorphic switch, growth and virulence of the
655 fungal wheat pathogen *Zymoseptoria tritici*. Mol Plant Pathol 21:124–138.

656 19. Han JW, Kim DY, Lee YJ, Choi YR, Kim B, Choi GJ, Han S-W, Kim H. 2020.
657 Transcription factor PdeR is involved in fungal development, metabolic change, and
658 pathogenesis of gray mold *Botrytis cinerea*. J Agric Food Chem 68:9171–9179.

659 20. Nitta M, Furukawa T, Shida Y, Mori K, Kuhara S, Morikawa Y, Ogasawara W. 2012. A
660 new Zn(II)2Cys6-type transcription factor BglR regulates β-glucosidase expression in
661 *Trichoderma reesei*. Fungal Genet Biol 49:388–397.

662 21. Xiong Y, Wu VW, Lubbe A, Qin L, Deng S, Kennedy M, Bauer D, Singan VR, Barry K,
663 Northen TR, Grigoriev IV, Glass NL. 2017. A fungal transcription factor essential for
664 starch degradation affects integration of carbon and nitrogen metabolism. PLOS
665 Genetics 13:e1006737.

666 22. Wu VW, Thieme N, Huberman LB, Dietschmann A, Kowbel DJ, Lee J, Calhoun S,
667 Singan VR, Lipzen A, Xiong Y, Monti R, Blow MJ, O'Malley RC, Grigoriev IV, Benz JP,

668 Glass NL. 2020. The regulatory and transcriptional landscape associated with carbon
669 utilization in a filamentous fungus. PNAS 117:6003–6013.

670 23. Gabriel R, Thieme N, Liu Q, Li F, Meyer LT, Harth S, Jecmenica M, Ramamurthy M,
671 Gorman J, Simmons BA, McCluskey K, Baker SE, Tian C, Schuerg T, Singer SW,
672 Fleißner A, Benz JP. 2021. The F-box protein gene exo-1 is a target for reverse
673 engineering enzyme hypersecretion in filamentous fungi. Proc Natl Acad Sci U S A
674 118:e2025689118.

675 24. Li J, Liu Q, Li J, Lin L, Li X, Zhang Y, Tian C. 2021. RCO-3 and COL-26 form an
676 external-to-internal module that regulates the dual-affinity glucose transport system in
677 *Neurospora crassa*. Biotechnology for Biofuels 14:33.

678 25. Hane JK, Paxman J, Jones DAB, Oliver RP, de Wit P. 2020. “CATAStrophy,” a
679 genome-informed trophic classification of filamentous plant pathogens – how many
680 different types of filamentous plant pathogens are there? Front Microbiol 10.

681 26. MacPherson S, Larochelle M, Turcotte B. 2006. A fungal family of transcriptional
682 regulators: the zinc cluster proteins. Microbiol Mol Biol Rev 70:583–604.

683 27. Schubert S, Popp C, Rogers PD, Morschhäuser J. 2011. Functional dissection of a
684 *Candida albicans* zinc cluster transcription factor, the multidrug resistance regulator
685 Mrr1. Eukaryotic Cell 10:1110–1121.

686 28. Erdős G, Dosztányi Z. 2020. Analyzing Protein Disorder with IUPred2A. Current
687 Protocols in Bioinformatics 70:e99.

688 29. Zhang Y, Liu T, Meyer CA, Eeckhoute J, Johnson DS, Bernstein BE, Nusbaum C,
689 Myers RM, Brown M, Li W, Liu XS. 2008. Model-based Analysis of ChIP-Seq (MACS).
690 Genome Biology 9:R137.

30. Ipcho SVS, Hane JK, Antoni EA, Ahren D, Henrissat B, Friesen TL, Solomon PS, Oliver RP. 2012. Transcriptome analysis of *Stagonospora nodorum*: gene models, effectors, metabolism and pantothenate dispensability. Mol Plant Pathol 13:531–545.

31. Siggers T, Duyzend MH, Reddy J, Khan S, Bulyk ML. 2011. Non-DNA-binding cofactors enhance DNA-binding specificity of a transcriptional regulatory complex. Mol Syst Biol 7:555.

32. Kojima T, Kunitake E, Ihara K, Kobayashi T, Nakano H. 2016. A robust analytical pipeline for genome-wide identification of the genes regulated by a transcription factor: combinatorial analysis performed using gSELEX-Seq and RNA-Seq. PLOS ONE 11:e0159011.

33. Zhao C, Waalwijk C, de Wit PJGM, van der Lee T, Tang D. 2011. EBR1, a novel Zn(2)Cys(6) transcription factor, affects virulence and apical dominance of the hyphal tip in *Fusarium graminearum*. Mol Plant Microbe Interact 24:1407–1418.

34. Jonkers W, Xayamongkhon H, Haas M, Olivain C, van der Does HC, Broz K, Rep M, Alabouvette C, Steinberg C, Kistler HC. 2014. *EBR1* genomic expansion and its role in virulence of *Fusarium* species. Environ Microbiol 16:1982–2003.

35. Adnan M, Zheng W, Islam W, Arif M, Abubakar YS, Wang Z, Lu G. 2017. Carbon catabolite repression in filamentous fungi. Int J Mol Sci 19:48.

36. John E, Singh KB, Oliver RP, Tan K-C. 2021. Transcription factor control of virulence in phytopathogenic fungi. Mol Plant Pathol 22:858–881.

37. Gomi K. 2019. Regulatory mechanisms for amylolytic gene expression in the koji mold *Aspergillus oryzae*. Bioscience, Biotechnology, and Biochemistry 83:1385–1401.

713 38. Wang P, Kojima T, Kobayashi T, Nakano H. 2012. Comprehensive analysis of the
714 DNA-binding specificity of an *Aspergillus nidulans* transcription factor, AmyR, using a
715 bead display system. Biosci Biotechnol Biochem 76:1128–1134.

716 39. Tani S, Katsuyama Y, Hayashi T, Suzuki H, Kato M, Gomi K, Kobayashi T, Tsukagoshi
717 N. 2001. Characterization of the *amyR* gene encoding a transcriptional activator for the
718 amylase genes in *Aspergillus nidulans*. Curr Genet 39:10–15.

719 40. Nakamura T, Maeda Y, Tanque N, Makita T, Kato M, Kobayashi T. 2006. Expression
720 profile of amylolytic genes in *Aspergillus nidulans*. Bioscience, Biotechnology, and
721 Biochemistry 70:2363–2370.

722 41. Marín-Menguiano M, Moreno-Sánchez I, Barrales RR, Fernández-Álvarez A, Ibeas JI.
723 2019. N-glycosylation of the protein disulfide isomerase Pdi1 ensures full *Ustilago*
724 *maydis* virulence. PLOS Pathogens 15:e1007687.

725 42. Lin S-Y, Chooi Y-H, Solomon PS. 2018. The global regulator of pathogenesis PnCon7
726 positively regulates *Tox3* effector gene expression through direct interaction in the
727 wheat pathogen *Parastagonospora nodorum*. Molecular Microbiology 109:78–90.

728 43. Craig JP, Coradetti ST, Starr TL, Glass NL. 2015. Direct target network of the
729 *Neurospora crassa* plant cell wall deconstruction regulators CLR-1, CLR-2, and XLR-1.
730 mBio 6.

731 44. IpCho SVS, Tan K-C, Koh G, Gummer J, Oliver RP, Trengove RD, Solomon PS. 2010.
732 The transcription factor StuA regulates central carbon metabolism, mycotoxin
733 production, and effector gene expression in the wheat pathogen *Stagonospora*
734 *nodorum*. Eukaryotic Cell 9:1100–1108.

735 45. Chooi Y-H, Zhang G, Hu J, Muria-Gonzalez MJ, Tran PN, Pettitt A, Maier AG, Barrow
736 RA, Solomon PS. 2017. Functional genomics-guided discovery of a light-activated

phytotoxin in the wheat pathogen *Parastagonospora nodorum* via pathway activation. Environ Microbiol 19:1975–1986.

46. Slattery M, Zhou T, Yang L, Dantas Machado AC, Gordân R, Rohs R. 2014. Absence of a simple code: how transcription factors read the genome. Trends in Biochemical Sciences 39:381–399.

47. Reiter F, Wienerroither S, Stark A. 2017. Combinatorial function of transcription factors and cofactors. Current Opinion in Genetics & Development 43:73–81.

48. Carey MF, Peterson CL, Smale ST. 2012. Confirming the Functional Importance of a Protein–DNA Interaction. Cold Spring Harb Protoc 2012:pdb.top070060.

49. Spivakov M. 2014. Spurious transcription factor binding: non-functional or genetically redundant? Bioessays 36:798–806.

50. Osterwalder M, Barozzi I, Tissières V, Fukuda-Yuzawa Y, Mannion BJ, Afzal SY, Lee EA, Zhu Y, Plajzer-Frick I, Pickle CS, Kato M, Garvin TH, Pham QT, Harrington AN, Akiyama JA, Afzal V, Lopez-Rios J, Dickel DE, Visel A, Pennacchio LA. 2018. Enhancer redundancy allows for phenotypic robustness in mammalian development. Nature 554:239–243.

51. Soyer JL, Ghalid ME, Glaser N, Ollivier B, Linglin J, Grandaubert J, Balesdent M-H, Connolly LR, Freitag M, Rouxel T, Fudal I. 2014. Epigenetic control of effector gene expression in the plant pathogenic fungus *Leptosphaeria maculans*. PLOS Genetics 10:e1004227.

52. Soyer JL, Möller M, Schotanus K, Connolly LR, Galazka JM, Freitag M, Stukenbrock EH. 2015. Chromatin analyses of *Zymoseptoria tritici*: methods for chromatin immunoprecipitation followed by high-throughput sequencing (ChIP-seq). Fungal Genet Biol 79:63–70.

761 53. Bewick AJ, Hofmeister BT, Powers RA, Mondo SJ, Grigoriev IV, James TY, Stajich JE,
762 Schmitz RJ. 2019. Diversity of cytosine methylation across the fungal tree of life. 3.
763 Nature Ecology & Evolution 3:479–490.

764 54. Syme RA, Tan K-C, Hane JK, Dodhia K, Stoll T, Hastie M, Furuki E, Ellwood SR,
765 Williams AH, Tan Y-F, Testa AC, Gorman JJ, Oliver RP. 2016. Comprehensive
766 annotation of the *Parastagonospora nodorum* reference genome using next-generation
767 genomics, transcriptomics and proteogenomics. PLOS ONE 11:e0147221.

768 55. Blum M, Chang H-Y, Chuguransky S, Grego T, Kandasaamy S, Mitchell A, Nuka G,
769 Paysan-Lafosse T, Qureshi M, Raj S, Richardson L, Salazar GA, Williams L, Bork P,
770 Bridge A, Gough J, Haft DH, Letunic I, Marchler-Bauer A, Mi H, Natale DA, Necci M,
771 Orengo CA, Pandurangan AP, Rivoire C, Sigrist CJA, Sillitoe I, Thanki N, Thomas PD,
772 Tosatto SCE, Wu CH, Bateman A, Finn RD. 2020. The InterPro protein families and
773 domains database: 20 years on. Nucleic Acids Res
774 https://doi.org/10.1093/nar/gkaa977.

775 56. Nguyen Ba AN, Pogoutse A, Provart N, Moses AM. 2009. NLStradamus: a simple
776 Hidden Markov Model for nuclear localization signal prediction. BMC Bioinformatics
777 10:202.

778 57. Andrews S. 2010. Babraham Bioinformatics - FastQC a quality control tool for high
779 throughput sequence data. https://www.bioinformatics.babraham.ac.uk/projects/fastqc/.
780 Retrieved 26 April 2021.

781 58. Martin M. 2011. Cutadapt removes adapter sequences from high-throughput
782 sequencing reads. 1. EMBnet.journal 17:10–12.

783 59. Bushnell B. 2016. BBMap. SourceForge. https://sourceforge.net/projects/bbmap/.
784 Retrieved 26 April 2021.

785 60. Li H. 2013. Aligning sequence reads, clone sequences and assembly contigs with
786 BWA-MEM. arXiv:13033997 [q-bio].

787 61. Li H, Handsaker B, Wysoker A, Fennell T, Ruan J, Homer N, Marth G, Abecasis G,
788 Durbin R, 1000 Genome Project Data Processing Subgroup. 2009. The sequence
789 alignment/map format and SAMtools. Bioinformatics 25:2078–2079.

790 62. Feng J, Liu T, Qin B, Zhang Y, Liu XS. 2012. Identifying ChIP-seq enrichment using
791 MACS. 9. Nat Protoc 7:1728–1740.

792 63. Gaspar JM. 2018. Improved peak-calling with MACS2. bioRxiv 496521.

793 64. Ramírez F, Ryan DP, Grüning B, Bhardwaj V, Kilpert F, Richter AS, Heyne S, Dündar
794 F, Manke T. 2016. deepTools2: a next generation web server for deep-sequencing data
795 analysis. Nucleic Acids Res 44:W160–W165.

796 65. Shao Z, Zhang Y, Yuan G-C, Orkin SH, Waxman DJ. 2012. MAnorm: a robust model
797 for quantitative comparison of ChIP-Seq data sets. Genome Biology 13:R16.

798 66. Bailey TL, Boden M, Buske FA, Frith M, Grant CE, Clementi L, Ren J, Li WW, Noble
799 WS. 2009. MEME SUITE: tools for motif discovery and searching. Nucleic Acids Res
800 37:W202-208.

801 67. Bailey TL, Elkan C. 1994. Fitting a mixture model by expectation maximization to
802 discover motifs in biopolymers. Proc Int Conf Intell Syst Mol Biol 2:28–36.

803 68. Bailey TL, Machanick P. 2012. Inferring direct DNA binding from ChIP-seq. Nucleic
804 Acids Res 40:e128–e128.

805 69. Grant CE, Bailey TL, Noble WS. 2011. FIMO: scanning for occurrences of a given
806 motif. Bioinformatics 27:1017–1018.

807 70. Armstrong RA. 2014. When to use the Bonferroni correction. Ophthalmic Physiol Opt
808 34:502–508.

809 71. Yu G, Wang L-G, He Q-Y. 2015. ChIPseeker: an R/Bioconductor package for ChIP
810 peak annotation, comparison and visualization. Bioinformatics 31:2382–2383.

811 72. Lin X, Tirichine L, Bowler C. 2012. Protocol: Chromatin immunoprecipitation (ChIP)
812 methodology to investigate histone modifications in two model diatom species. Plant
813 Methods 8:48.

814 73. Bursteinas B, Britto R, Bely B, Auchincloss A, Rivoire C, Redaschi N, O'Donovan C,
815 Martin MJ. 2016. Minimizing proteome redundancy in the UniProt Knowledgebase.
816 Database : J Biol Databases Curation 2016.

817 74. Yu G, Wang L-G, Han Y, He Q-Y. 2012. clusterProfiler: an R package for comparing
818 biological themes among gene clusters. OMICS: A Journal of Integrative Biology
819 16:284–287.

820

821

7. Tables

Table 1. Rationale for the investigation of novel transcription factors (TFs) in this study

TF investigated	Involvement	Virulence-associated orthologues [A]
PnPro1 (SNOG_3490)	Directly-positively regulated by PnPf2	*AbPro1* (*Ab*), *MoPRO1* (*Mo*), *GzZC232* (*Fg*), *UvPro1* (*Uv*)
PnAda1 (SNOG_04486)	Directly-positively regulated by PnPf2	*GzbZIP001* (*Fg*), *FpAda1* (*Fp*)
SNOG_08237	Directly-positively regulated by PnPf2	*CoHox1* (*Co*)
SNOG_08565	Shared ancestral lineage with PnPf2 orthologues	-
PnEbr1 (SNOG_03067)	Co-expressed with *PnPf2*, *ToxA*, *Tox1* and *Tox3* during infection	*EBR1* (*Fg*), *EBR1* (*Fo*), *MoCod2* and *Cnf2* (*Mo*)
PnCreA (SNOG_13619)	Enriched CreA-binding motif (22) in PnPf2-regulated gene promoters	*CreA* (*Af*), *Cre1* (*Fo*), *CreA* (*Pe*)

[A] Putative orthologues were inferred by cross-referencing a previous TF-orthology analysis and literature review (15, 36). Abbreviations: *Ab; Alternaria brassicicola*, *Af; Aspergillus flavus*, *Co; Colletotrichum orbiculare, Fg; Fusarium graminearum, Fo; Fusarium oxysporum, Fp; Fusarium pseudograminearum, Mo; Magnaporthe oryzae*, *Pe; Penicillium expansum*.

Table 2. Overview of the strains referenced in this study [A]

Strain ID	Description [B]
SN15	Wildtype *P. nodorum* reference isolate
pf2ko	Original *PnPf2* deletion mutant (12, 13)
pf2_KO	*PnPf2* deletion mutant to facilitate targeted complementation
Pf2_OE	*PnPf2* overexpression (*pGpdA* promoter)
Pf2-GFP	*PnPf2* with *GFP* tag, native promoter
Pf2-GFP_OE	*PnPf2* with *GFP* tag, overexpression promoter
Pf2-HA	*PnPf2* with 3x*HA* tag, native promoter
Pf2-HA_OE	*PnPf2* with 3x*HA* tag, overexpression promoter
pf2-HA_KO	*PnPf2* coding sequence replaced with 3x*HA* tag
CreA_OE	*PnCreA* overexpression (*pGpdA* promoter)
creA_KO	*PnCreA* deletion mutant
CreA_Ec	*PnCreA* ectopically-integrated construct
SN15-*GFP*	SN15 constitutively expressing *GFP*
pTef1-dTom	SN15 constitutively expressing *dTomato* (defined locus)
p15417_M1M2	SN15 expressing *dTomato* (defined locus) SNOG_15417 promoter, no mutations
p15417_m1M2	SN15 expressing *dTomato* (defined locus) SNOG_15417 promoter, M1 mutated
p15417_M1m2	SN15 expressing *dTomato* (defined locus) SNOG_15417 promoter, M2 mutated
p15417_m1m2	SN15 expressing *dTomato* (defined locus) SNOG_15417 promoter, M1+2 mutated
pro1_KO	*PnPro1* deletion mutant
Pro1_comp	*PnPro1* complemented in *pro1_KO* background
ada1_KO	*PnAda1* deletion mutant
Ada1_comp	*PnAda1* complemented in *ada1_KO* background
08237_KO	SNOG_08237 deletion mutant
08237_comp	SNOG_08237 complemented in *08237_KO* background
08565_KO	SNOG_08565 deletion mutant
08565_comp	SNOG_08565 complemented in *08565_KO* background
ebr1_KO	*PnEbr1* deletion mutant
Ebr1_Ec	*PnEbr1* ectopically-integrated construct

[A] Strains are listed in corresponding order to the detailed description of their generation in Text S3.

[B] Abbreviations: GFP – Green fluorescent protein, HA – Haemagglutinin, M1 – Motif1, M2 – Motif 2.

8. Figures

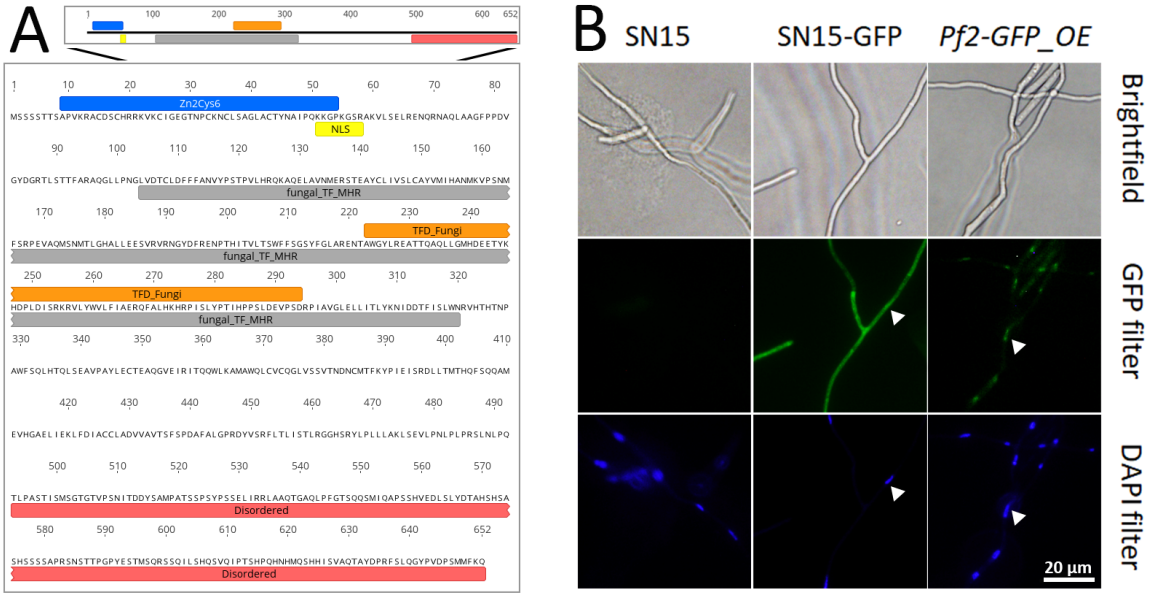

Fig. 1 PnPf2 domain analysis and cellular localisation. A) Predicted domains and features identified in the 652 amino acid PnPf2 protein sequence typical of a Zn_2Cys_6 transcription factor (TF). The region corresponding to the N-terminal Zn_2Cys_6 DNA binding domain (Zn_2Cys_6 - Interpro IPR001138) is depicted in blue and the nuclear localisation signal (NLS) is in yellow. The fungal transcription factor domain (TFD_fungi - Interpro IPR007219) corresponds to orange within the 'middle homology region' (fungal_TF_MHR - Conserved Domain Database CD12148) depicted in grey. A C-terminal disordered protein region lacking secondary structure was identified that corresponds to the red bar. B) Epifluorescence microscopy depicting nuclear localisation of the GFP-tagged PnPf2 translational fusion specific to the *Pf2-GFP_OE* overexpression strain, in contrast to the wildtype (SN15) and the positive control strain expressing cytoplasmic GFP (SN15-*GFP*). Arrows indicate the corresponding locations of fungal nuclei under the respective filters determined by DAPI staining of a germinated pycnidiospore. A fluorescence signal was not detected in the *Pf2-GFP*

853 strain, where expression was driven by the native *PnPf2* promoter, indicating PnPf2
854 accumulates at relatively low abundance.
855
856
857

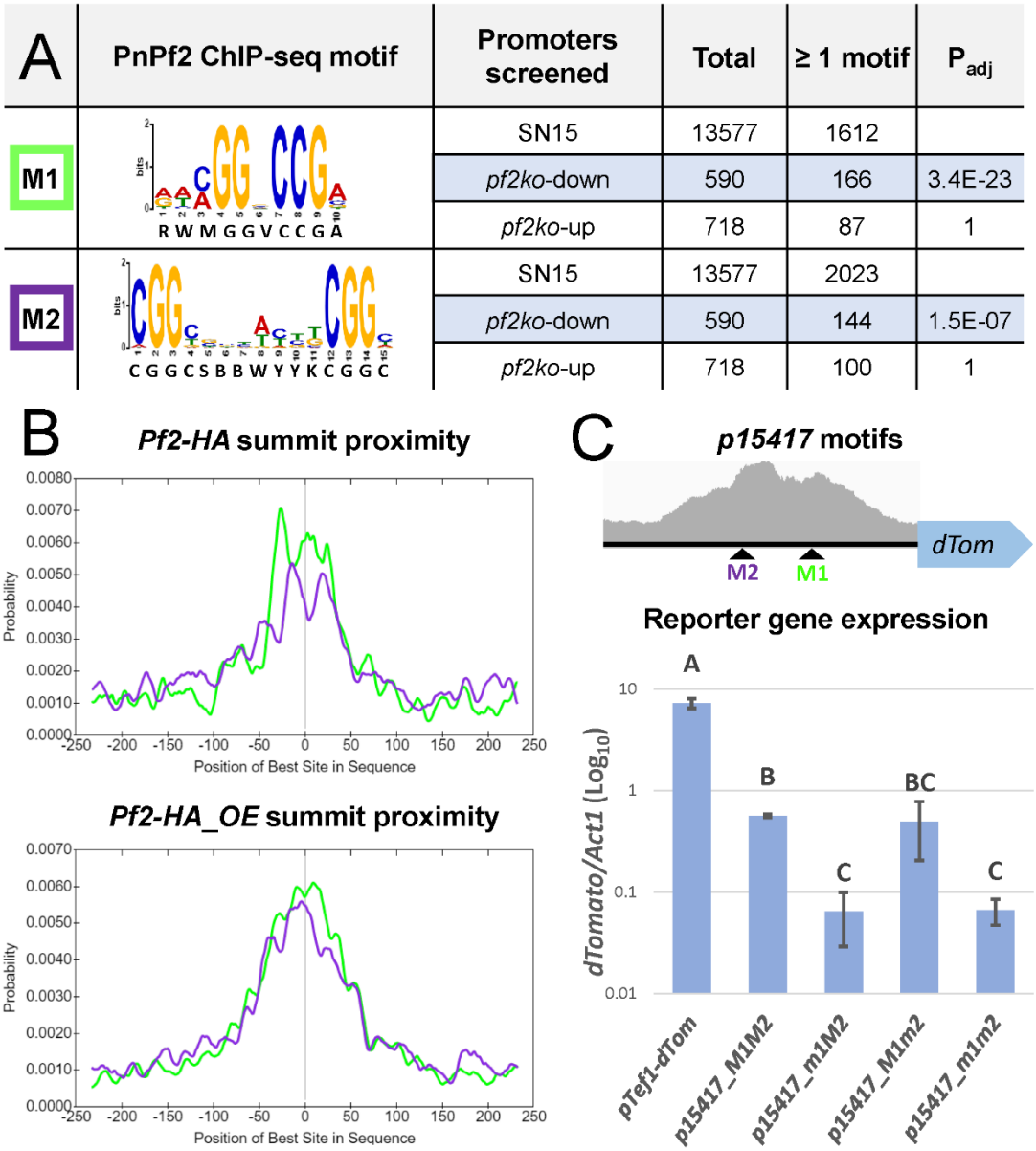

858

859 **Fig. 2** Identification of PnPf2 regulatory element motifs. **A)** The M1 motif (5'-
860 RWMGGVCCGA-3') and M2 motif (5'-CGGCSBBWYYKCGGC-3') were modelled
861 from the merged set of *Pf2-HA* and *Pf2-HA_OE* sample ChIP-seq peak regions. Their
862 detection (≥ 1 occurrence) in the promoters of PnPf2 positively (*pf2ko*-down) or
863 negatively (*pf2ko*-up) regulated gene promoters (13) are indicated relative to all SN15
864 promoters. The P_{adj} value reflects the test for significant enrichment (Fisher's test with
865 Bonferroni $P_{adj} < 0.01$), where both motifs were enriched in the *pf2ko*-down genes
866 relative to SN15. **B)** The position of motif occurrences relative to ChIP-seq summits,

867 demonstrating their higher likelihood at close proximity to the best estimate of PnPf2-
868 DNA binding loci. **C)** Gene expression analysis assessing the effect of M1 and M2
869 motif mutation in *P. nodorum in situ*. The motif loci within a ChIP-seq peak in the
870 SNOG_15417 gene promoter region (*p15417*) are depicted. The *dTomato* reporter
871 gene was fused to a constitutive promoter control (*pTef1-dTom*) or the SNOG_15417
872 gene promoter (*p15417_M1M2*) in the *P. nodorum* background. The motifs were also
873 mutated through substitution of the respective 'CGG' triplets, alone or in combination
874 (*p15417_m1M2*, *p15417_M1m2* and *p15417_m1m2*). The strains *p15417_m1M2* and
875 *p15417_m1m2* where M1 had been mutated exhibited significantly reduced
876 expression relative to the non-mutated promoter in *p15417_M1M2*. This suggested
877 PnPf2 regulatory activity had been impaired following M1 mutation but not M2 mutation
878 in *p15417*. Letters indicate statistically distinct groupings by ANOVA with Tukey's-HSD
879 ($P<0.05$).
880

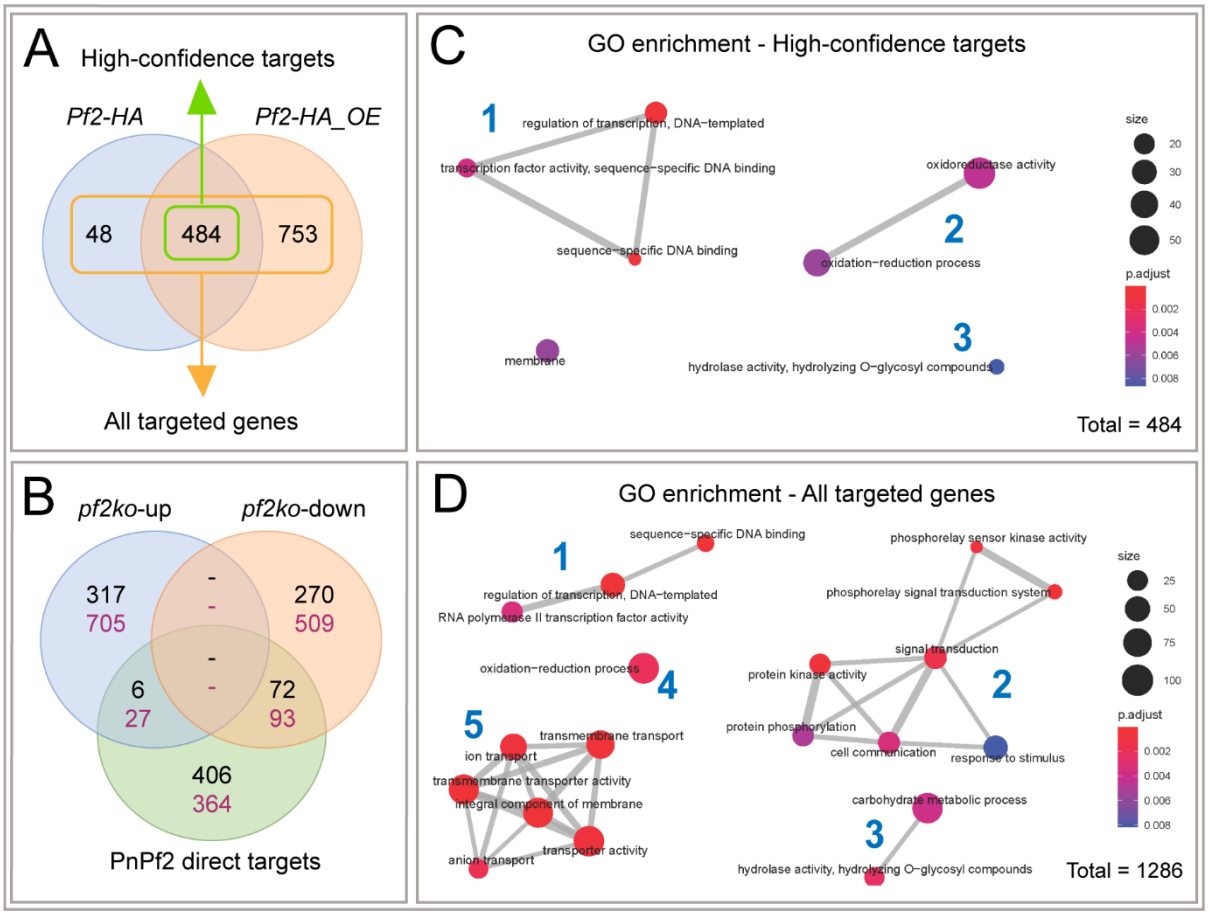

Fig. 3 Gene expression and gene-ontology (GO) analysis of PnPf2 direct targets. **A)** Overview of the genes targeted by PnPf2 in their promoter region based on the respective *Pf2-HA* and *Pf2-HA_OE* ChIP-seq datasets. There were 484 genes considered high-confidence PnPf2 targets among the 1286 putative targets from either construct. **B)** The high-confidence targets in comparison with their expression pattern in the *pf2ko* deletion mutant. Black numbers correspond to the *in vitro* growth conditions replicated for ChIP-seq sample preparation while purple numbers also encompass differentially expressed genes during early infection. The greater overlap with PnPf2 positively-regulated (*pf2ko*-down - 72 genes) than repressed (*pf2ko*-up - 6 genes) suggested PnPf2 predominantly functions as a positive regulator of gene expression. **C-D)** A summary of significantly-enriched GO terms among PnPf2-targeted genes. The high-confidence (*Pf2-HA* and *Pf2-HA_OE*) and total identified

894 targets (*Pf2-HA* or *Pf2-HA_OE*) are both displayed for comparison. Bubble sizes are
895 proportionate to gene counts, colours to the enrichment test *P* values and the lines
896 between bubbles to the total shared terms. Numbers in blue indicate connected gene
897 networks representing transcription factors [number 1], redox molecules [2],
898 carbohydrate-active enzymes [3], cell-signalling molecules [4], and trans-membrane
899 transporters [5].

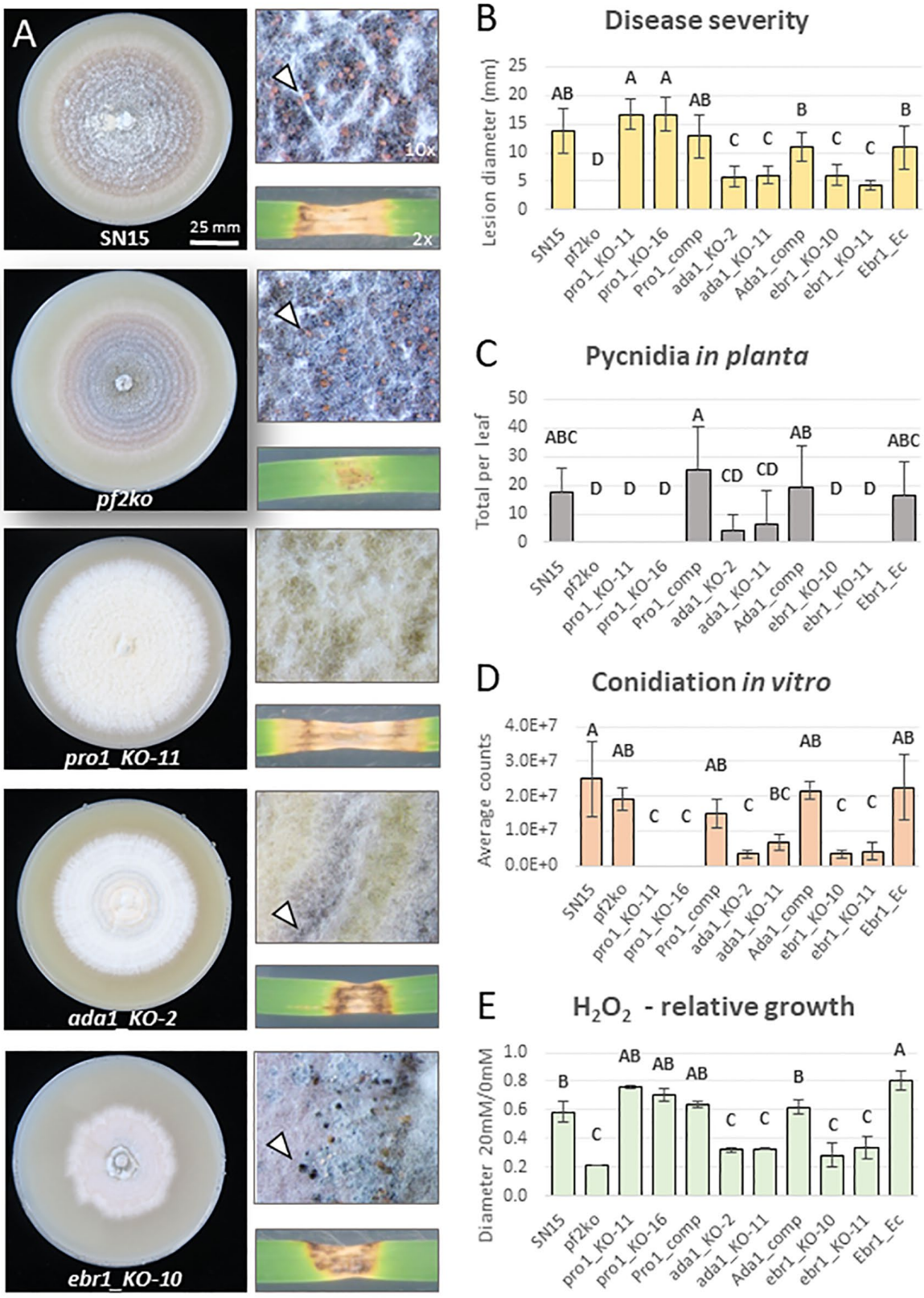

902 **Fig. 4** Phenotypic assessment of transcription factor (TF) gene deletion mutants. **A)**
903 Representative images after 12 days of growth on nutrient-rich agar (V8PDA) and
904 infection on detached wheat leaves (cv. Halberd). Arrows demonstrate pycnidia if they
905 were detected in the respective mutants. **B)** Average lesion sizes representing disease
906 severity. **C)** Pycnidia counts, a measure of pathogenic fitness following the infection.
907 **D)** Average conidial (pycnidiospore) counts on V8PDA. **E)** Growth inhibition on 20mM
908 H_2O_2 relative to 0mM on minimal medium agar. Letters indicate statistically distinct
909 groupings by ANOVA with Tukey's-HSD ($P<0.05$).
910

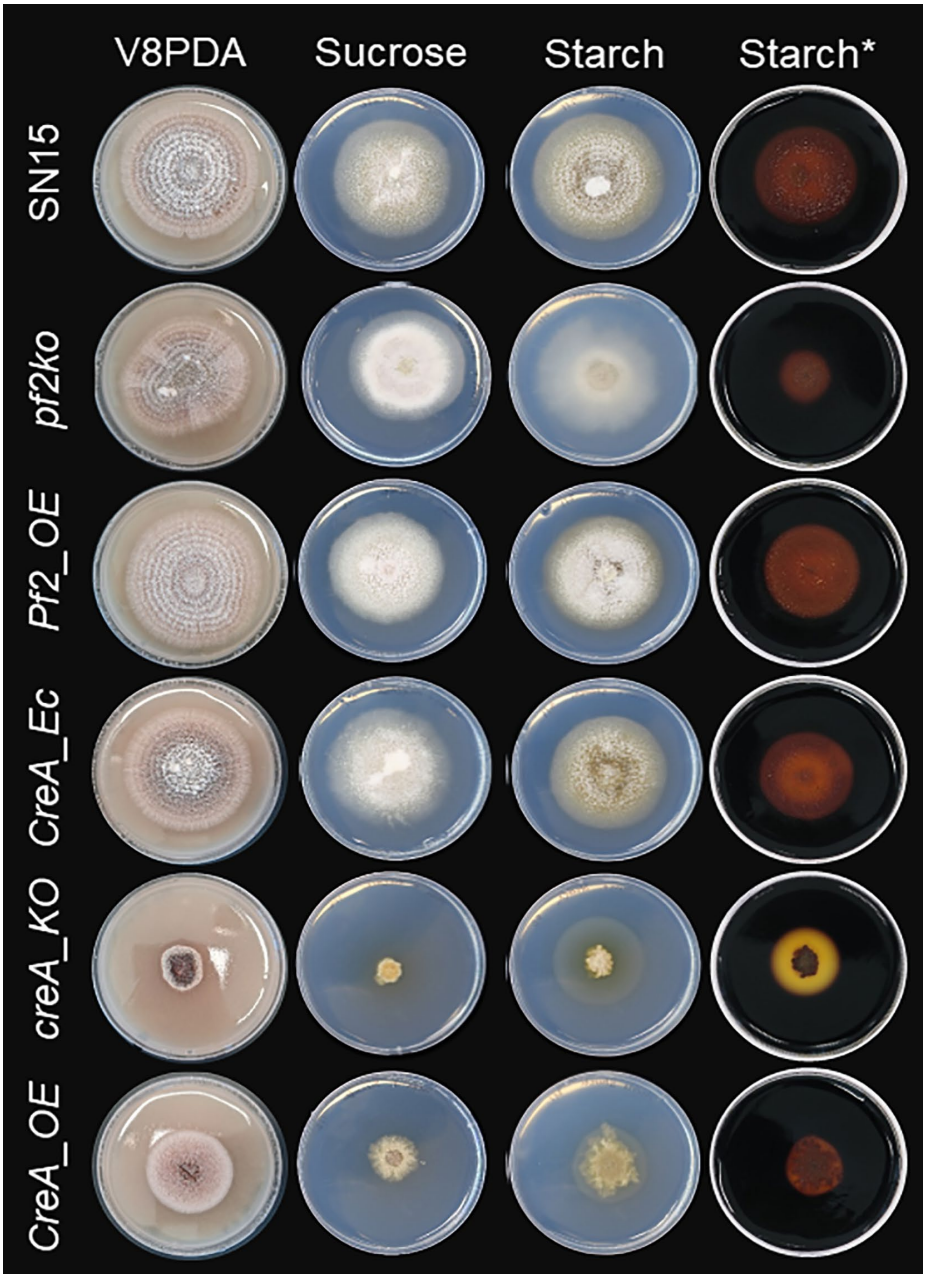

911

912 **Fig. 5** Assessment of *PnPf2* and *PnCreA* mutant growth on different substrates.
913 Images following 12 days of growth on nutrient-rich V8PDA and minimal-medium agar
914 with a primary (sucrose) or secondary (starch) carbon source. Wildtype SN15 and the
915 respective mutants are listed on each row. The capacity to fully utilise starch was
916 enhanced in the *creA_KO* mutant despite growth defects, suggesting impaired carbon-
917 catabolite repression. Starch utilisation was moderately reduced in the *pf2ko* mutant.
918 *Post-stained with Lugol's iodine to assist visualisation of starch hydrolysis.

919

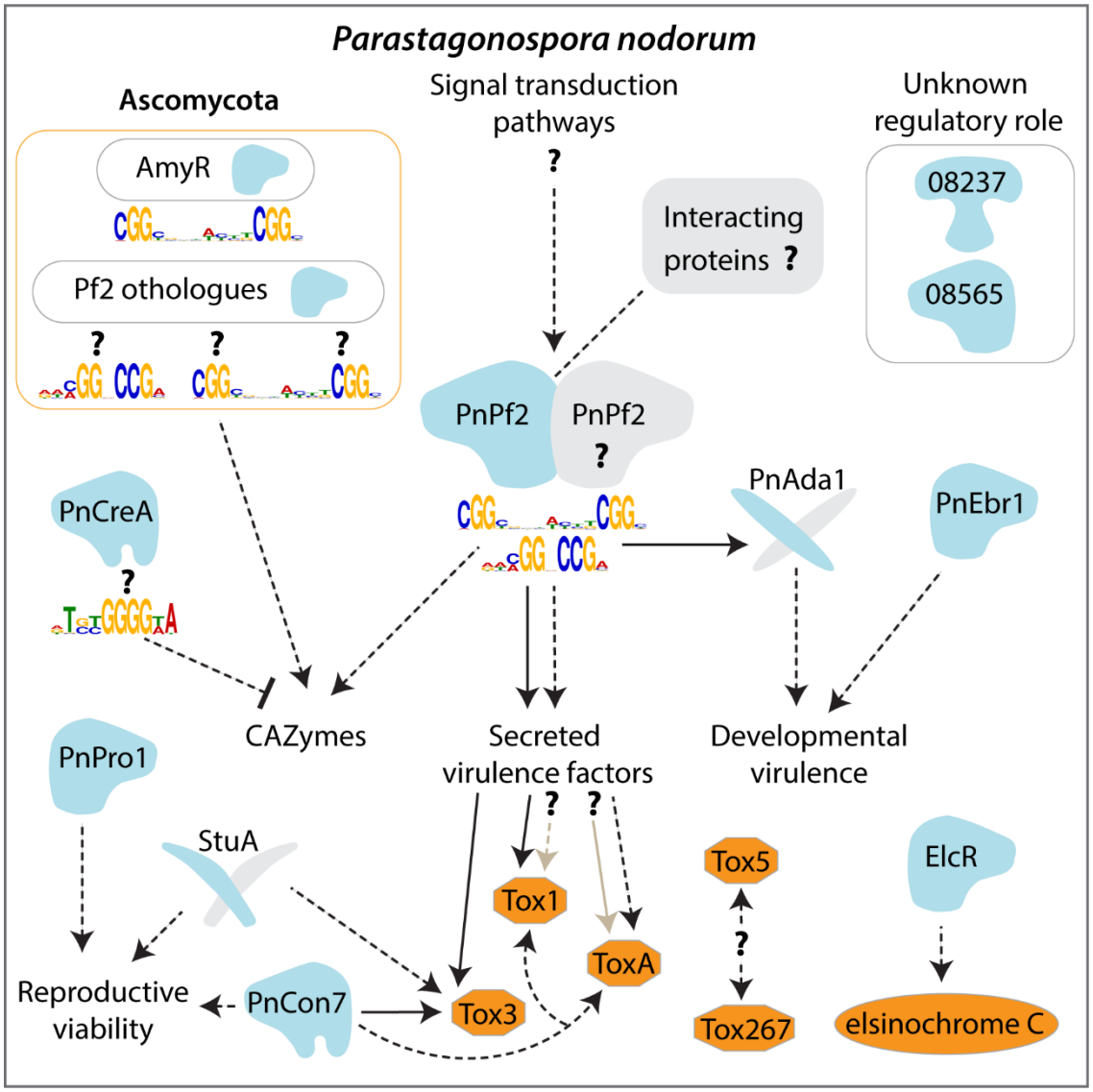

Fig. 6 The proposed model of the PnPf2-centred regulatory network in the virulence of *P. nodorum*. The Pf2 taxonomic orthologues and AmyR regulators in the Ascomycota fungi (discussed in the main text) are presented for context regarding the two PnPf2 regulatory motifs described in this study. Transcription factors (TFs) and virulence factors that are cloned and characterised in *P. nodorum* are depicted (blue and orange shapes respectively; grey shapes indicate putative interacting proteins). Dashed arrows show where gene regulation occurs and solid arrows represent direct regulation. Question marks are presented where evidence is tentative and requires validation. PnPf2 controls the expression of key virulence

930 factors. The effector *Tox3* is directly regulated and *ToxA*, based on promoter-motif
931 and gene expression data, is likely a direct target during plant infection. PnPf2 also
932 directly targets the *Tox1* promoter as a possible enhancer while regulators of *Tox267*
933 and *Tox5* require investigation. Carbohydrate-active enzymes (CAZymes) are also
934 regulated by PnPf2, with a subset putatively repressed by PnCreA for which no
935 distinct role in virulence has been established. Developmental virulence, such as
936 oxidative stress tolerance and hyphal growth, were processes attributed in this study
937 to the PnPf2 targets PnAda1 and PnEbr1. PnPro1 and StuA (44) are essential for
938 reproduction by sporulation, while no distinct role was identified for the putative TFs
939 encoded by SNOG_08237 and SNOG_08565. Elsewhere, PnCon7 has been
940 reported to regulate effector expression but is an essential viability factor, while
941 production of a phytotoxic metabolite elsinochrome C is controlled by the pathway-
942 specific ElcR gene-cluster TF (45, 42).
943
944

9. Supplemental item legends

Text S1 Chromatin immunoprecipitation (ChIP) strain assessment and overview of ChIP-seq/ChIP-qPCR.

Text S2 Supplemental transcription factor mutant phenotype assessment.

Text S3 Supplemental materials and methods.

Fig. S1 A depiction of the PnPf2 targeting of characterised effector genes in *P. nodorum* SN15. The *Pf2-HA* and *Pf2-HA_OE* ChIP-seq read peaks are presented at the *Tox3*, *Tox1*, *ToxA* and *Tox267* promoters. Peak summits were evident in the *Tox3* and *Tox1* promoters. Red dots represent instances of the M1 motif (5'-RWMGGVCCGA-3') and blue dots M2 (5'-CGGCSBBWYYKCGGC-3').

Fig. S2 A heatmap depiction of *Parastagonospora nodorum* SN15 hierarchical cluster analysis. Clustering was based on microarray gene-expression data during infection (*in planta*) or axenic (*in vitro*) growth obtained from a previous study (30). Clusters were cut into the 10 most distant clusters to identify genes co-expressed with *PnPf2*, *ToxA*, *Tox1* and *Tox3*, which included the Zn_2Cys_6 transcription factor *PnEbr1* (SNOG_03037) therefore investigated in this study.

File S1 A spreadsheet detailing the genomic coordinates for ChIP-seq peak regions [columns A-D], the respective summit loci [E], the pileup height of the mapped reads [F] and the summit $-Log_{10}$(Q-values) representing the difference of ChIP reads relative to the input control sample [G]. The *Pf2-HA* strain encompasses columns A-G and the *Pf2-HA_OE* strain encompasses column H-N. Also included are the genomic coordinates for the peak regions obtained by merging the overlapping regions from the *Pf2-HA* and *Pf2-HA_OE* samples using MAnorm (65) [O-S].

File S2 A spreadsheet of PnPf2 regulation data across the *P. nodorum* SN15 genome for the respective annotated genes [column A]. Listed are whether ChIP-seq

promoter summits were called from the *Pf2-HA* and *Pf2-HA_OE* samples [B-C], whether the enriched PnPf2 target motifs [D-E] or the putative PnCreA motif [G] were present in the gene promoter regions, and whether the gene was also down-regulated in the *pf2ko* mutant [G]. Also listed are the functional annotations [G-M]; whether the gene was classed as effector-like [H], a TF [I], the associated GO IDs/terms [J-K] and Interpro domain information [L-M]. The final columns list the respective gene expression data for *pf2ko* compared with SN15 either *in vitro* (*iv*) or *in planta* (*ip*) [13-22]. *Information indicated was derived from Jones et al. (2019) for comparative purposes.

File S3 A spreadsheet compilation of the primers used in this study organised by their general use [column 1] with the primer ID and sequence [2-3] and descriptions for their use [4-5]. Highlighted in italics are restriction enzyme recognition sites, in bold are overlapping regions used in cloning and in red are sites for incorporating single nucleotide changes during cloning.